frontiers | Frontiers in Energy Research

TYPE Original Research
PUBLISHED 15 November 2023
DOI 10.3389/fenrg.2023.1293267

OPEN ACCESS

EDITED BY
Michael Howard Meylan,
The University of Newcastle, Australia

REVIEWED BY
Sahaj Saxena,
Thapar Institute of Engineering and Technology, India
Omveer Singh,
Gautam Buddha University, India

*CORRESPONDENCE
Safeer Ullah,
dr_safeer_ullah@quaideazam.edu.pk

RECEIVED 12 September 2023
ACCEPTED 26 October 2023
PUBLISHED 15 November 2023

CITATION
Hua L-G, Ali A, Ullah S, Hafeez G, Zaidi MM and Jun LJ (2023), Robust finite-time integral terminal sliding mode control design for maximum power extraction of PMSG-based standalone wind energy system.
Front. Energy Res. 11:1293267.
doi: 10.3389/fenrg.2023.1293267

Robust finite-time integral terminal sliding mode control design for maximum power extraction of PMSG-based standalone wind energy system

Lyu-Guang Hua[1], Ammar Ali[2], Safeer Ullah[3]*, Ghulam Hafeez[4], Monji Mohamed Zaidi[5] and Liu Jun Jun[1]

[1]Power China Huadong Engineering Co. Ltd., Hangzhou, China, [2]Department of Electrical Engineering, Bahria University, Islamabad, Pakistan, [3]Department of Electrical Engineering, Quaid-e-Azam College of Engineering and Technology, Sahiwal, Pakistan, [4]Department of Electrical Engineering, University of Engineering and Technology, Mardan, Pakistan, [5]Department of Electrical Engineering, College of Engineering, King Khalid University, Abha, Saudi Arabia

This paper introduces a novel control strategy called Finite-time Integral Terminal Sliding Mode Control (FITSMC), explicitly designed for a permanent-magnet synchronous generator (PMSG)-based standalone Wind Energy Conversion System (WECS). The primary objective of the FITSMC strategy is to regulate the operation of the wind turbine efficiently and maximize power extraction from the WECS. To achieve this, the system is driven onto a sliding surface within a predefined terminal time, ensuring rapid convergence and overall stability. An important advantage of the FITSMC strategy is its ability to maintain a standalone wind power system close to the maximum power point, even under varying wind conditions and load changes. In addition, the controller demonstrates robustness against uncertainties and disturbances, making it highly suitable for real-world applications. Extensive simulations and analyses have been conducted to validate the effectiveness of the proposed FITSMC. The results show a superior control performance compared to traditional methods. Consequently, the FITSMC strategy represents a promising advancement in control techniques for standalone wind power systems, providing an efficient and reliable approach for harnessing power from wind energy.

KEYWORDS

finite-time integral terminal SMC, maximum power point tracking (M.P.P.T), permanent magnet synchronous generator (PMSG), wind turbine (WT), wind energy system (WES)

1 Introduction

Increasing global population and economic development have led to the establishment of new power plants to meet rising energy demands. However, the energy crisis, higher oil prices, and climate change underscore the significance of Renewable Energy Resources (RESs) (Anjum et al., 2022). Governments worldwide are now prioritizing effective, sustainable, and environmentally friendly renewable energy systems. Renewable energy sources, such as wind and solar energy systems, have grown substantially, catering to energy

demand while considering environmental concerns and the finite nature of nonrenewable energy sources.

Wind energy, being green and environmentally friendly, offers a promising solution for reducing the dependence on fossil fuels and mitigating their negative impacts (Dali et al., 2021). Technological advancements in wind energy have played a crucial role in power system integration, control theory, aerodynamic designs, mechanical systems, and power electronic converters. Extracting the maximum power (MP) from wind power systems (WPS) is a crucial research area. Wind speed sensorless Maximum Power Point Tracking (MPPT) control has gained considerable attention for optimizing power extraction without physically altering the wind turbine or system components. Various techniques and design considerations have been explored for WPSs (Cullen, 2000; Raj and Kumar, 2018; Costanzo et al., 2019).

In the existing literature, robust controllers have been developed and studied for extracting maximum power P_{max} from the wind (Aboudrar et al., 2019; Syahputra and Soesanti, 2019; Cheikh et al., 2020; Saidi et al., 2020; Khan et al., 2021; Alam et al., 2022; Khan et al., 2022; Chand et al., 2023). Some studies have focused on reactive power and maximum inverter power extraction without wind speed sensors (Abdullah et al., 2012), whereas others have explored adaptive MPPT schemes and improved control techniques for grid-connected wind turbines (Jaramillo-Lopez et al., 2016; Pan and Shao, 2020; Hawkins and McIntyre, 2021). Furthermore, numerous other MPPT control approaches have been developed for wind energy systems, enhancing their efficiency and reliability (Chu et al., 2014). These techniques fall into three categories: conventional methods, population-based algorithms, and artificial intelligence (AI) strategies. However, maintaining the maximum power output across all wind speeds remains challenging because of inherent nonlinear characteristics (Tafticht et al., 2006; Soetedjo et al., 2011). Various estimation techniques have been employed, but some may introduce vulnerabilities owing to modelling inaccuracies (Lee et al., 2009; Ullah et al., 2023; Ullah et al., 2021).

Sliding mode control (SMC) is widely considered as a robust nonlinear MPPT control strategy. However, the chattering and asymptotic convergence issues have led to criticism. To address these challenges, a solution has been presented in the form of an integral sliding mode control (ISMC) strategy (Ullah S. et al., 2020), which enhances robustness and diminishes chattering. Despite its advantages, tuning the switching gain parameter in the ISMC remains challenging. In the study described in (Wang et al., 2019), a novel adaptive Lyapunov stability-based backstepping control technique was proposed for MPPT of a variable-speed PMSG-WECS. The control strategy is designed to provide robustness against uncertainties even without prior knowledge of the upper bounds. Overall, the backstepping technique offers a fast dynamic response and robustness. However, it also presents challenges regarding design complexity, real-time implementation feasibility, and the possibility of controlling the signal chattering. Overcoming these limitations and effectively applying backstepping control in practical systems require careful consideration and precise tuning.

This study contributes significantly to three key areas. 1) Introducing an FITSMC methodology for a fixed-pitch, variable-speed, 3 kW standalone PMSG-WECS in the presence of measurement noise to optimize power output by tracking the MPP. The FITSMC method is novel in the aforesaid system due to its innovative control approach, addressing nonlinear dynamics and uncertainties. This ensures rapid and accurate control of wind energy systems, enhancing performance and reliability, even under variable wind conditions. The FITSMC reduces mechanical and electrical stresses, extends component lifetimes, and promotes system sustainability. This adoption in PMSG-WECS contributes significantly to renewable energy and control systems, advancing wind energy integration into the power grid for a cleaner, sustainable energy transition. 2) Transforming the dynamical model of the considered PMSG-WECS system into a control-convenient input-output form serves as the basis for designing the control methodology. 3) Validation of the efficacy and performance of the proposed control technique through extensive simulation experiments in MATLAB. The obtained results are meticulously compared with established literature results, solidifying the evidence of the effectiveness and advantages of the proposed control design.

The remainder of this paper is organized as follows. Section 2 presents the equivalent model of a PMSG-WECS and provides the essential mathematical preliminaries. In Section 3, a control algorithm is derived to achieve the maximum power extraction from the PV array, ensuring optimal efficiency. A discussion of the simulation results, which show the robustness of the proposed control law, can be found in Section 4. Finally, Section 5 offers concluding remarks, summarizing the findings and contributions of this study.

1.1 Mathematical notations and variables

The analysis of the PMSG-WECS involves a wide array of constants and parameters. These include critical factors such as the mechanical power output of the turbine (P_M), wind speed expressed in meters per second (V_{wind}), air density (ρ), and area swept by the turbine blades (A). Additionally, the conversion of the wind turbine rotor power is governed by the wind turbine rotor power conversion coefficient (Γ_{wind}) and the blade radius is represented by $\mathcal{R}_t$. In this context, variables of significant importance include the tip speed ratio (λ), blade pitch angle (β), and optimal tip speed ratio (λ_{opt}). The analysis also considers the maximum power coefficient ($C_{p_{\max}}$) and other parameters relevant to the PMSG-WECS.

Turning to the modeling of the PMSG itself, a meticulous examination of the electrical properties was conducted. This includes variables such as the stator resistance ($\mathcal{R}_s$), permanent magnet flux variables (ω_m and ϕ_m), rotor inductances along the d-axis and q-axis (L_d and L_q), and rotor inductance (L), particularly for non-salient PMSG configurations. Furthermore, the analysis explores variables, including the currents along the d-axis (i_d) and q-axis (i_q), as well as the high-speed shaft speed (ω_h). Various constants (d_1, d_2, d_3) are also incorporated into the modeling process of the PMSG-WECS system. The system introduces a set of state variables, specifically x_1, x_2, and x_3, which effectively represent

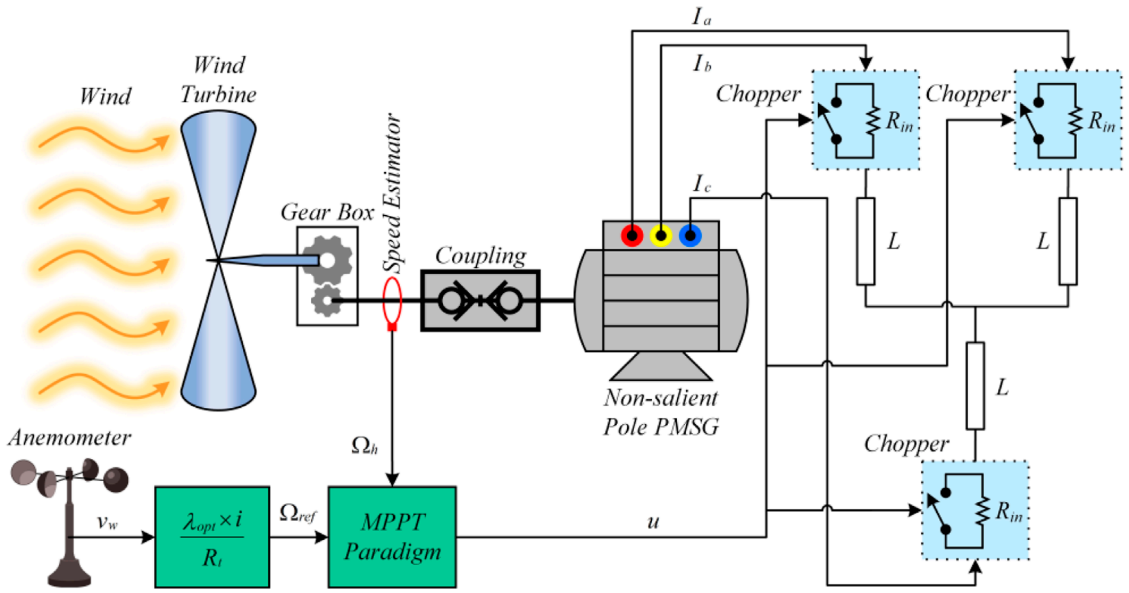

FIGURE 1
Schematic diagram depicting the configuration of the PMSG-WECS.

the state of the PMSG-WECS system. These state variables evolve dynamically over time, guided by the state vector field ($f(x)$). Within this framework, we also consider a matrix of smooth functions ($g(x)$) and output function ($h(x)$). Here, the Lie derivatives ($\mathcal{L}_f$ and $\mathcal{L}_g$) play a significant role in investigating the dynamics of the system.

Control strategies played an integral role in the analysis. A control input (u) is introduced into the system, and the design incorporates constants such as α_3, β_3, and γ_3), which are of paramount importance in the realm of sliding mode control. Elements, such as the sliding surface (σ_3) and tracking error (e_3), are fundamental components of the control framework. The derivative of the sliding surface ($\dot{\sigma}_3$) provides valuable insights into the behavior of the system. The design also incorporates control inputs for strong reachability factors ($u_{q(equ)}$) and discrete control ($u_{q(dis)}$) along with pertinent control constants ($\mathcal{K}_c$ and $\mathcal{K}_d$). Throughout the analysis, specific indexes are judiciously applied to signify optimal values (opt) and variables associated with sliding mode control (3) to enhance clarity and facilitate a deeper understanding of the subject matter.

2 Dynamical modeling of the standalone PMSG-WECS

This section describes the dynamical modelling of the system under study. As illustrated in Figure 1, the system schematic encompasses essential components such as the power electronic converter, gearbox, variable speed wind turbine (VSWT), PMSG coupled with the VSWT, and load. We aim to examine the behavior of the system and the interplay between these components, ultimately formulating mathematical models that facilitate control design and performance assessment.

2.1 Dynamical modeling of the wind turbine

The following set of mathematical equations describes a wind turbine with fixed-pitch configuration Zafran et al. (2020); Khan et al. (2021):

$$P_M = \frac{1}{2}\rho A V_{wind}^3 = \Gamma_{wind}\ \omega_t \tag{1}$$

where P_M represents the turbine output mechanical power, V_{wind} is the wind speed in m/s, ρ denotes the air density, and A is the area swept by the blades. The parameter Γ_{wind} is defined as:

$$\Gamma_{wind} = 0.5\rho\pi\mathcal{R}_t^3 V_w^2 C_T(\lambda) \tag{2}$$

The dynamic modelling of the variable-speed standalone PMSG-WECS involves key parameters such as the blade radius $\mathcal{R}_t$ in meters, wind turbine rotor power conversion coefficient $C_T(\lambda)$, and tip-speed ratio $\lambda = \frac{\mathcal{R}_t\omega_t}{V_{wind}}$. Additionally, the air density ρ (usually 1.25 kg/m^3 at 100°C at sea level), power coefficient C_p, blade pitch angle β, and the optimal tip-speed ratio $\lambda_{opt} = 7$ play vital roles in maximizing power extraction under varying wind speeds. To achieve optimal power extraction under varying wind conditions, the blade pitch angle β is set to 0, resulting in a maximum power coefficient $C_{pmax} = 0.47$ at the corresponding tip speed ratio λ_{nom} or λ_{opt}. The mechanical power produced by the wind turbine at different

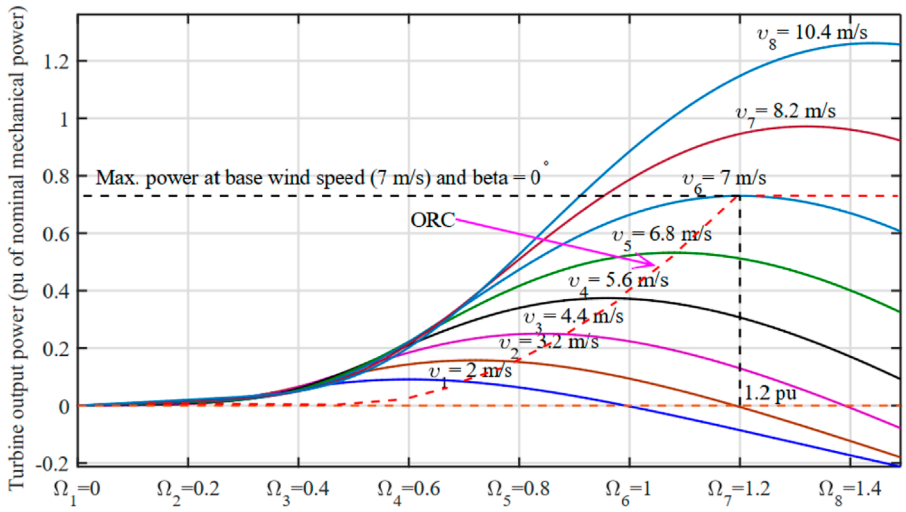

FIGURE 2
Turbine Speed vs. Turbine Output Mechanical Power.

wind speeds is illustrated in Figure 2. At each wind speed, a distinct maximum power point P_{mopt} is evident, which collectively defines the optimal regime characteristic (ORC). The ORC designates a specific operating region in which the WECS efficiently extracts the maximum energy, even under varying wind conditions. The MPPT control strategy ensures that the wind turbine operates within the designated ORC despite fluctuations in wind speed. The MPPT control scheme continuously adjusts the turbine operation, aligns it with the ORC, and maximizes the power extraction efficiency.

For the variable speed wind turbine reported in Munteanu et al. (2009), C_p can be determined by the numerical following approximation while considering $\beta = 0^0$:

$$\begin{aligned} C_p(\lambda) =& 0 + 0.0061\lambda - 0.0013\lambda^2 + 0.0081\lambda^3 - 0.000974\lambda^4 \\ &+ 0.0000654\lambda^5 + 0.00000130\lambda^6 - 0.000000454\lambda^7 \end{aligned} \tag{3}$$

The VSWT is optimized to track the maximum value of C_p, denoted as $C_{p_{max}}$, which occurs at a specific tip speed ratio λ_{opt}. By maintaining the tip-speed ratio at its optimal value λ_{opt}, VSWT can effectively extract the maximum wind power Chand et al. (2023); Majout et al. (2022); Zafran et al. (2020).

In this study, the critical wind turbine parameters include the air density ρ (set to 1.25 kg/m^3), gears ratio or transmission ratio i (equal to 7), blade radius $\mathcal{R}_t$ (measuring 2.5 m), maximum power coefficient $C_{p_{max}}$ (equal to 0.47), optimal tip-speed ratio λ_{opt} (valued at 7), and high-speed shaft inertia $\mathcal{J}_h$ (measured as 0.0552 kg$\cdot$m^2) Chand et al. (2023); Majout et al. (2022); Khan et al. (2022, 2021); Ullah A. et al. (2020); Alam et al. (2022).

Having discussed the essential rotor blade parameters, the next section briefly explores them.

2.2 Modelling of the permanent magnet synchronous generator

A simplified dq model of the three-phase PMSG in the dq-reference frame, neglecting the zero components, is utilized for the dynamical modelling of the variable speed standalone WECS. The dq-axis voltages represent output variables. The following set of differential equations describes the PMSG model.

$$\left.\begin{aligned} v_d &= \mathcal{R}_a i_d + L_d \frac{d}{dt} i_d - L_q i_q \\ v_q &= \mathcal{R}_a i_q + L_q \frac{d}{dt} i_q + \left(L_d i_d + \phi_m\right) \end{aligned}\right\} \tag{4}$$

where v_d and v_q represent the voltages along the dq-axes, $\mathcal{R}_s$ is the stator resistance, ω_m is the permanent magnet flux, and ϕ_m is the maximum magnetic flux. The rotor inductances L_d and L_q are assumed to be equal (i.e., $L_d = L_q = L$) for a non-salient PMSG. The PMSG-WECS system has three states: i_d, i_q, and ω_h. To design a controller, the PMSG equations are reformulated as nonlinear dynamic equations as follows:

$$\left.\begin{aligned} \left(L_d + L_{ch}\right)\dot{x}_1 &= -\mathcal{R}_s x_1 + p\left(L_q - L_{ch}\right)x_2 x_3 - \mathcal{R}_{ini} x_1 \\ \left(L_q + L_{ch}\right)\dot{x}_2 &= p\left(L_q + L_{ch}\right)\phi_m x_3 - \mathcal{R}_s x_2 \\ -p\left(L_d + L_{ch}\right)x_1 x_3 &- \mathcal{R}_{ini} x_2 \\ \mathcal{J}_h \dot{x}_3 &= \frac{d_1 v_w^{\,2}}{i} + \frac{d_2 v_w x_3}{i^3} + \frac{d_3 x_3^{\,2}}{i^3} - p\phi_m x_2 \end{aligned}\right\} \tag{5}$$

where p denotes the number of pole pairs, $\mathcal{J}_h$ represents the moment of inertia of the PMSG high-speed shaft, and $\mathcal{R}_{ini}$ and L_{ch} refer to the resistance and inductance of the load, respectively.

The system, characterized by its input vector $u = \mathcal{R}_{ini} \in \mathbb{R}^m$, output vector $y = h(x) \in \mathbb{R}^l$, and state vector $x \in \mathbb{R}^n$, can be presented in a general form as follows:

$$\left.\begin{aligned} \dot{x} &= f(x) + g(x)\,u \\ y &= h(x) \end{aligned}\right\} \tag{6}$$

The nonlinear smooth state vector field $f(x) \in \mathbb{R}^n$ with a matrix of smooth functions $g(x) \in \mathbb{R}^{n\times m}$ can be expressed as:

$$f(x) = \begin{bmatrix} \dfrac{-\mathcal{R}_s x_1 + p\left(L_q - L_{ch}\right)x_2 x_3}{\left(L_d + L_{ch}\right)} \\ \dfrac{-\mathcal{R}_s x_2 - p\left(L_d + L_{ch}\right)x_1 x_3}{\left(L_q + L_{ch}\right)} + p\phi_m x_3 \\ \left(\dfrac{d_1 v_w^2}{i} + \dfrac{d_2 v_w x_3}{i^3} + \dfrac{d_3 x_3^2}{i^3} - p\phi_m x_2\right)\dfrac{1}{\mathcal{J}_h} \end{bmatrix};$$
$$g(x) = \begin{bmatrix} \dfrac{-x_1}{\left(L_d + L_{ch}\right)} \\ \dfrac{-x_2}{\left(L_q + L_{ch}\right)} \\ 0 \end{bmatrix}; x = \begin{bmatrix} i_d \\ i_q \\ \omega_h \end{bmatrix} \tag{7}$$

Now, by utilizing Equations 6, 7, we can represent the PMSG-WECS model in state-space form as follows:

$$\begin{bmatrix} \dot{x}_1 \\ \dot{x}_2 \\ \dot{x}_3 \end{bmatrix} = \begin{bmatrix} -k_1 x_1 - k_2 x_2 x_3 \\ -l_1 x_2 - l_2 x_1 x_3 + l_3 x_3 \\ -m_1 - m_2 x_3 - m_3 x_3^2 - m_4 x_2 \end{bmatrix} + \begin{bmatrix} -k_3 x_1 \\ -l_4 x_2 \\ 0 \end{bmatrix} u$$
$$y = h(x) = [0 \quad 0 \quad 1]\begin{bmatrix} x_1 \\ x_2 \\ x_3 \end{bmatrix} \tag{8}$$

where $k_1 = \frac{\mathcal{R}_s}{(L_d+L_{ch})}$, $k_2 = -\frac{p(L_q-L_{ch})}{(L_d+L_{ch})}$, $k_3 = \frac{1}{(L_d+L_{ch})}$, $l_1 = \frac{\mathcal{R}_s}{(L_q+L_{ch})}$, $l_2 = \frac{p(L_d+L_{ch})}{(L_q+L_{ch})}$, $l_3 = p\phi_m$, $l_4 = \frac{1}{(L_q+L_{ch})}$, $m_1 = -\frac{d_1 v_w^2}{i\mathcal{J}_h}$, $m_2 = -\frac{d_2 v_w}{i^3\mathcal{J}_h}$, $m_3 = -\frac{d_3}{i^3\mathcal{J}_h}$ and $m_4 = \frac{p\phi_m}{\mathcal{J}_h}$.

To determine the relative degree r of the considered system, one can ensure the satisfaction of the following equation is satisfied:

$$\mathcal{L}_g\mathcal{L}_f^{r-1}h(x) \neq 0 \quad \text{for} \quad r = 1, 2, 3, \ldots \tag{9}$$

where $\mathcal{L}_g$ and $\mathcal{L}_f$ are the Lie derivatives of the nonlinear functions $g(x)$ and $f(x)$ with respect to the system state vector x, respectively, and $h(x)$ is a output function of the observer state vector x.

By implementing (Eq. 9), the following expressions are obtained.

$$\begin{aligned} \mathcal{L}_g h(x) &= 0 \\ \mathcal{L}_f h(x) &= -m_1 - m_2 x_3 - m_3 x_3^2 - m_4 x_2 \\ \mathcal{L}_g\mathcal{L}_f h(x) &= l_4 m_4 x_2 \neq 0 \end{aligned} \tag{10}$$

This confirms that the studied system had a relative degree of 2. Subsequently, we transform the system into an input-output form in the following subsection and design the control input u accordingly.

2.3 Input-output form transformation

Prior to expressing the system in a standard canonical form (normal form or input-output form), a coordinate transformation for the system is required. This transformation is performed as follows:

$$\mathfrak{z} = \left[\mathfrak{z}_1, \quad \mathcal{L}_f h(x), \quad \mathcal{L}_f^2 h(x), \ \ldots, \ \mathcal{L}_f^{r-1} h(x)\right] \tag{11}$$

where

$$\left.\begin{aligned} \mathfrak{z}_1 &= x_3 \\ \mathfrak{z}_2 = \mathcal{L}_f h(x) &= -m_1 - m_2 x_3 - m_3 x_3^2 - m_4 x_2 \\ \mathfrak{z}_3 = \mathcal{L}_f^2 h(x) &= \frac{x_1}{x_2} \end{aligned}\right\} \tag{12}$$

and the inverse coordinates transform are

$$\left.\begin{aligned} x_1 &= \mathfrak{z}_3\left(m_1 - \mathfrak{z}_2 - m_2\mathfrak{z}_1 - m_3\mathfrak{z}_1^2\right)/m_4 \\ x_2 &= \left(m_1 - \mathfrak{z}_2 - m_2\mathfrak{z}_1 - m_3\mathfrak{z}_1^2\right)/m_4 \\ x_3 &= \mathfrak{z}_1 \end{aligned}\right\} \tag{13}$$

Now, the system dynamics in the $\mathfrak{z}$-domain can be written as

$$\begin{aligned} \dot{\mathfrak{z}}_1 &= \dot{x}_3 = \mathfrak{z}_2 \\ \dot{\mathfrak{z}}_2 &= \mathcal{L}_f^2 h(x) + \mathcal{L}_g\mathcal{L}_f h(x)\, u \end{aligned} \tag{14}$$

where $\mathcal{L}_f^2 h(x) = -m_4 f_2 - (m_2 + 2m_3 x_3) f_3$ and $\mathcal{L}_g\mathcal{L}_f h(x) = l_4 m_4 x_2$. Hence, the linearized model of the system in the $\mathfrak{z}$ domain is

$$\left.\begin{aligned} \begin{bmatrix} \dot{\mathfrak{z}}_1 \\ \dot{\mathfrak{z}}_2 \end{bmatrix} &= \begin{bmatrix} 0 & 1 \\ 0 & 0 \end{bmatrix}\begin{bmatrix} \mathfrak{z}_1 \\ \mathfrak{z}_2 \end{bmatrix} + \begin{bmatrix} 0 \\ 1 \end{bmatrix} u \\ y &= \begin{bmatrix} 1 & 0 \end{bmatrix}\begin{bmatrix} \mathfrak{z}_1 \\ \mathfrak{z}_2 \end{bmatrix} \end{aligned}\right\} \tag{15}$$

Note that the control input u will be designed with the help of a fast integral terminal SMC scheme, and we check the stability of the system's third internal dynamic state in the following subsection.

2.4 Zero-dynamic stability investigation of the system

After all the calculations and transformation into a $\mathfrak{z}$-coordinate system, we achieved the third internal dynamic state of the system, that is

$$\begin{aligned} \dot{\mathfrak{z}}_3 = &\frac{m_4}{m_1}\left(-\frac{k_1\mathfrak{z}_3 m_1}{m_4} - \frac{k_2\mathfrak{z}_1 m_1}{m_4} - \frac{k_3\mathfrak{z}_3 m_1 u}{m_4}\right) \\ &+ \frac{\mathfrak{z}_3 m_4}{m_1}\left(\frac{l_1 m_1}{m_4} + \frac{l_2 m_1\mathfrak{z}_3\mathfrak{z}_1}{m_4} - l_3\mathfrak{z}_1 + \frac{l_4 m_1 u}{m_4}\right) \end{aligned} \tag{16}$$

To analyze the stability of the zero-dynamic state, we set the following variables to zero: $\mathfrak{z}_1 = \mathfrak{z}_2 = u = 0$. By simplifying Equation 16, we get

$$\dot{\mathfrak{z}}_3 = -\mathfrak{z}_3(k_1 - l_1) \tag{17}$$

where $k_1 > l_1$, so

$$\dot{\mathfrak{z}}_3 = -k_1\ \mathfrak{z}_3 \tag{18}$$

The zero-dynamic state remains stable for all $k_1 > l_1$, where k_1 is a positive integer.

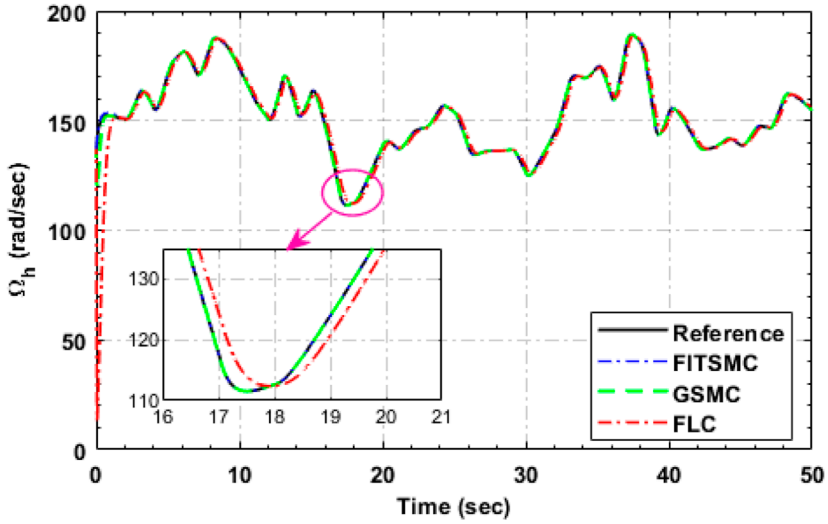

FIGURE 3
Tracking performance of high-speed shaft rotational speed.

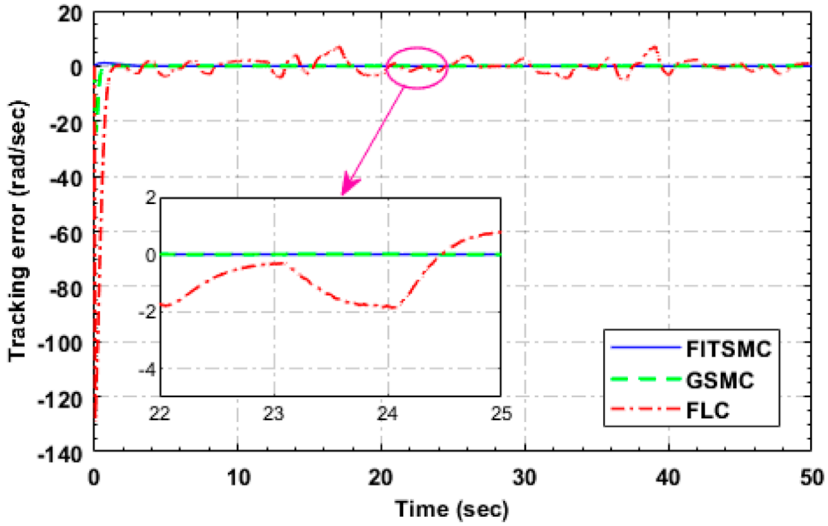

FIGURE 4
Error in high-speed shaft rotational speed tracking.

In the next step, we will design a control algorithm to adjust the duty cycle and maximize power extraction from the wind turbine system.

3 Finite-time sliding mode controller for maximum power point tracking of WECS

This section introduces a novel nonlinear fast integral terminal SMC strategy to regulate the generator speed of a PMSG in a WECS. The primary goal of the proposed control law is to optimize the chop resistance, ensuring that the generator operates at its optimal speed and achieves the maximum power extraction from the PMSG.

3.1 Control design

The first step in the control design is to precisely track the reference speed. To accomplish this, we define the tracking error as

$$e_{\mathfrak{z}} = \mathfrak{z}_1 - \mathfrak{z}_d \tag{19}$$

where z_d represents the desired or reference value for the variable z. By taking the double derivative of the error, we obtain

$$\begin{aligned} \dot{e}_{\mathfrak{z}} &= \mathfrak{z}_2 - \dot{\mathfrak{z}}_d \\ \ddot{e}_{\mathfrak{z}} &= \dot{\mathfrak{z}}_2 - \ddot{\mathfrak{z}}_d \end{aligned} \tag{20}$$

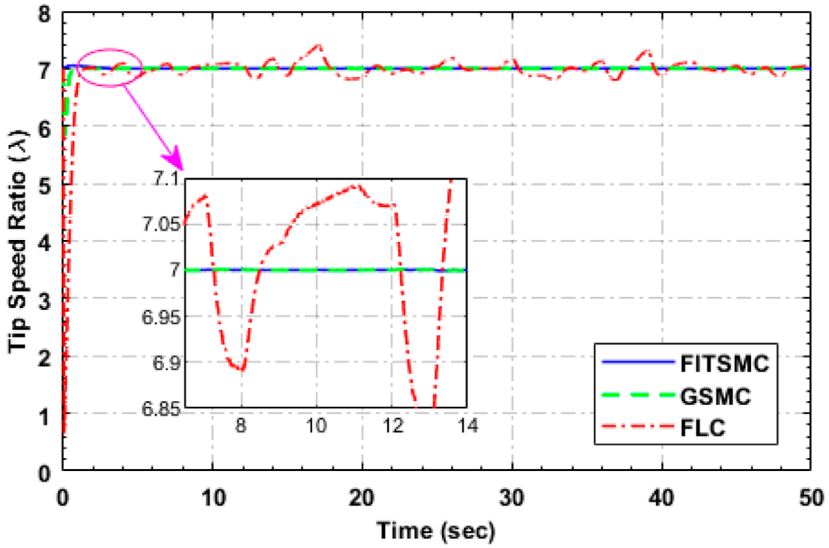

FIGURE 5
Performance of tip speed ratio.

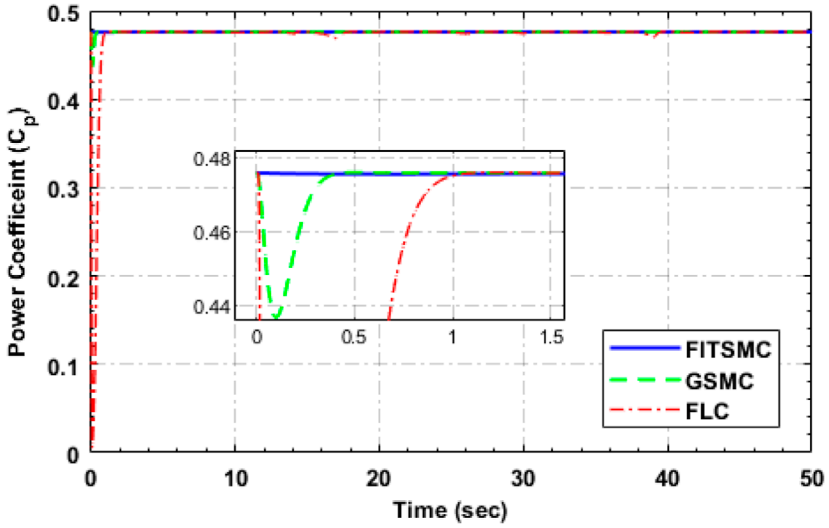

FIGURE 6
Power conversion coefficient performance.

The finite-time integral terminal sliding surface is defined as

$$\sigma_{\mathfrak{z}} = \dot{e}_{\mathfrak{z}} + \alpha_{\mathfrak{z}} e_{\mathfrak{z}} + \beta_{\mathfrak{z}} \int_0^t |e_{\mathfrak{z}}|^{\gamma_{\mathfrak{z}}} sign\left(e_{\mathfrak{z}}\right) d\tau \tag{21}$$

Here, $\alpha_{\mathfrak{z}}$ and $\beta_{\mathfrak{z}}$ are positive design constants, and $\gamma_{\mathfrak{z}} = \frac{q_{\mathfrak{z}}}{p_{\mathfrak{z}}}$, where $q_{\mathfrak{z}}$ and $p_{\mathfrak{z}}$ are positive odd integers. The first derivative of the sliding surface is expressed as

$$\begin{aligned} \dot{\sigma}_{\mathfrak{z}} &= \ddot{e}_{\mathfrak{z}} + \alpha_{\mathfrak{z}} \dot{e}_{\mathfrak{z}} + \beta_{\mathfrak{z}} |e_{\mathfrak{z}}|^{\gamma_{\mathfrak{z}}} sign\left(e_{\mathfrak{z}}\right) \\ \dot{\sigma}_{\mathfrak{z}} &= \dot{\mathfrak{z}}_2 - \ddot{\mathfrak{z}}_d + \alpha_{\mathfrak{z}} \left(\mathfrak{z}_2 - \dot{\mathfrak{z}}_d\right) + \beta_{\mathfrak{z}} |\mathfrak{z}_1 - \mathfrak{z}_d|^{\gamma_{\mathfrak{z}}} sign\left(\mathfrak{z}_1 - \mathfrak{z}_d\right) \end{aligned} \tag{22}$$

By utilizing the values of $\dot{\mathfrak{z}}_1$ and $\dot{\mathfrak{z}}_2$, Eq. 23 can be derived as

$$\begin{aligned} \dot{\sigma}_{\mathfrak{z}} =& \mathcal{L}_f^2 h(x) + \mathcal{L}_g \mathcal{L}_f h(x) u_{(q)} + \Delta - \ddot{\mathfrak{z}}_d + \alpha_{\mathfrak{z}} \left(\mathfrak{z}_2 - \dot{\mathfrak{z}}_d\right) \\ &+ \beta_{\mathfrak{z}} |\mathfrak{z}_1 - \mathfrak{z}_d|^{\gamma_{\mathfrak{z}}} sign\left(\mathfrak{z}_1 - \mathfrak{z}_d\right) \end{aligned} \tag{23}$$

Assuming $\dot{\sigma}_{\mathfrak{z}} = 0$, the control input $u_{q(equ)}$ can be calculated as follows:

$$\begin{aligned} u_{q(equ)} =& \frac{1}{\mathcal{L}_g \mathcal{L}_f h(x)} \left[-\mathcal{L}_f^2 h(x) + \ddot{\mathfrak{z}}_d - \alpha_{\mathfrak{z}} \left(\mathfrak{z}_2 - \dot{\mathfrak{z}}_d\right) \right. \\ & \left. -\beta_{\mathfrak{z}} |\mathfrak{z}_1 - \mathfrak{z}_d|^{\gamma_{\mathfrak{z}}} sign\left(\mathfrak{z}_1 - \mathfrak{z}_d\right) \right] \end{aligned} \tag{24}$$

The strong reachability factor is defined as

$$u_{q(dis)} = -\mathcal{K}_c \sigma_{\mathfrak{z}} - \mathcal{K}_d sign\left(\sigma_{\mathfrak{z}}\right) \tag{25}$$

Hence, the overall control input becomes

$$u_{\mathfrak{z}} = \frac{1}{\mathcal{L}_g \mathcal{L}_f h(x)} \left[-\mathcal{L}_f^2 h(x) + \ddot{\mathfrak{z}}_d - \alpha_{\mathfrak{z}} \left(\mathfrak{z}_2 - \dot{\mathfrak{z}}_d \right) - \beta_{\mathfrak{z}} \left| \mathfrak{z}_1 - \mathfrak{z}_d \right|^{\gamma_{\mathfrak{z}}} sign\left(\mathfrak{z}_1 - \mathfrak{z}_d \right) \right] - \mathcal{K}_c \sigma_{\mathfrak{z}} - \mathcal{K}_d sign\left(\sigma_{\mathfrak{z}} \right) \tag{26}$$

3.2 Stability analysis

To demonstrate the stability of the PMSG-WECS under the FITSMC, we use a Lyapunov-based stability analysis and use the following Lyapunov function to prove the enforcement of the sliding mode:

$$\Lambda_{\mathfrak{z}} = \frac{1}{2} \sigma_{\mathfrak{z}}^2 \tag{27}$$

Taking the derivative of $\Lambda_{\mathfrak{z}}$, we have that

$$\dot{\Lambda}_{\mathfrak{z}} = \sigma_{\mathfrak{z}} \dot{\sigma}_{\mathfrak{z}} \tag{28}$$

By substituting the value of $\dot{\sigma}_{\mathfrak{z}}$ from Equation 23 and simplifying it, we obtain

$$\dot{\Lambda}_{\mathfrak{z}} = \sigma_{\mathfrak{z}} \left(\mathcal{L}_f^2 h(x) + \mathcal{L}_g \mathcal{L}_f h(x) u_{(\mathfrak{z})} + \Delta - \ddot{\mathfrak{z}}_d + \alpha_{\mathfrak{z}} \left(\mathfrak{z}_2 - \dot{\mathfrak{z}}_d \right) + \beta_{\mathfrak{z}} \left| \mathfrak{z}_1 - \mathfrak{z}_d \right|^{\gamma_{\mathfrak{z}}} sign\left(\mathfrak{z}_1 - \mathfrak{z}_d \right) \right) \tag{29}$$

After substituting the controller $u_{(q)}$ value and simplifying it, we obtain

$$\dot{\Lambda}_{\mathfrak{z}} = -\mathcal{L}_g \mathcal{L}_f h(x) \mathcal{K}_c \sigma_{\mathfrak{z}}^2 - \mathcal{L}_g \mathcal{L}_f h(x) \mathcal{K}_d sign\left(\sigma_{\mathfrak{z}} \right) \sigma_{\mathfrak{z}} + (\Delta) \sigma_{\mathfrak{z}} \tag{30}$$

Because $sign(\sigma_{\mathfrak{z}}) \sigma_{\mathfrak{z}} = \left| \sigma_{\mathfrak{z}} \right|$, Equation 30 becomes

$$\dot{\Lambda}_{\mathfrak{z}} \le -\mathcal{L}_g \mathcal{L}_f h(x) \mathcal{K}_c \sigma_{\mathfrak{z}}^2 - \mathcal{L}_g \mathcal{L}_f h(x) \mathcal{K}_d \left| \sigma_{\mathfrak{z}} \right| + |\Delta| \left| \sigma_{\mathfrak{z}} \right| \tag{31}$$

$$\dot{\Lambda}_{\mathfrak{z}} \le -\mathcal{L}_g \mathcal{L}_f h(x) \mathcal{K}_c \sigma_{\mathfrak{z}}^2 - \left| \sigma_{\mathfrak{z}} \right| \left(\mathcal{L}_g \mathcal{L}_f h(x) \mathcal{K}_d - |\Delta| \right) \tag{32}$$

The uncertainty term $\eta_{\mathfrak{z}}$ is defined as follows:

$$\mathcal{L}_g \mathcal{L}_f h(x) \mathcal{K}_d - |\Delta| \ge \eta_{\mathfrak{z}} \tag{33}$$

We can rewrite inequality (Eq. 32) as:

$$\dot{\Lambda}_{\mathfrak{z}} \le -\mathcal{L}_g \mathcal{L}_f h(x) \mathcal{K}_c \sigma_{\mathfrak{z}}^2 - \left| \sigma_{\mathfrak{z}} \right| \eta_{\mathfrak{z}} \tag{34}$$

To solve the Lyapunov function for the sliding surface, we have

$$\left| \sigma_{\mathfrak{z}} \right| = \sqrt{2 \Lambda_{\mathfrak{z}}} \tag{35}$$

By substituting $\left| \sigma_{\mathfrak{z}} \right|$ with $\sqrt{2 \Lambda_{\mathfrak{z}}}$ in Eq. 34, we have

$$\begin{aligned} \dot{\Lambda}_{\mathfrak{z}} &\le -\mathcal{L}_g \mathcal{L}_f h(x) \mathcal{K}_c 2 \Lambda_{\mathfrak{z}} - \eta_{\mathfrak{z}} \sqrt{2 \Lambda_{\mathfrak{z}}} \\ \dot{\Lambda}_{\mathfrak{z}} &+ \mathcal{L}_g \mathcal{L}_f h(x) \mathcal{K}_c 2 \Lambda_{\mathfrak{z}} + \eta_{\mathfrak{z}} \sqrt{2} \sqrt{\Lambda_{\mathfrak{z}}} \le 0 \\ \dot{\Lambda}_{\mathfrak{z}} &+ \bar{\mathcal{K}} \Lambda_{\mathfrak{z}} + \bar{\eta}_{\mathfrak{z}} \sqrt{\Lambda_{\mathfrak{z}}} \le 0 \end{aligned} \tag{36}$$

where $\bar{\mathcal{K}}_c = \mathcal{L}_g \mathcal{L}_f h(x) \mathcal{K}_c 2$ and $\bar{\eta}_{\mathfrak{z}} = \sqrt{2} \eta_{\mathfrak{z}}$.

$$T_f \le \frac{1}{2 \bar{\mathcal{K}}_c} \ln \left(\frac{\bar{\mathcal{K}}_c \sqrt{\Lambda_{\mathfrak{z}}} \left(\sigma_{\mathfrak{z}}(0) \right) + \bar{\eta}_{\mathfrak{z}}}{\bar{\eta}_{\mathfrak{z}}} \right) \tag{37}$$

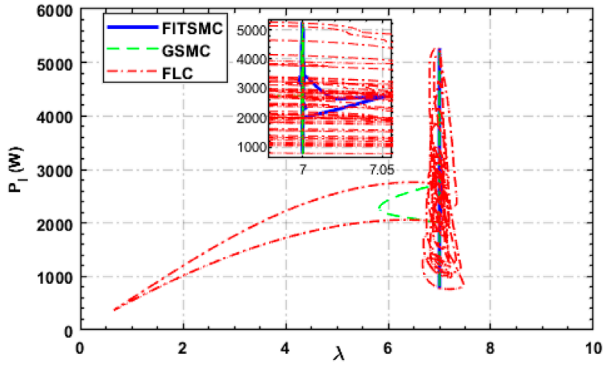

FIGURE 7
Relationship between wind turbine mechanical power and tip speed ratio.

The above inequality signifies rapid finite-time convergence, meaning that, as time progresses, $\Lambda_{\mathfrak{z}}$ tends to zero at a fast rate. Consequently, the sliding surface converged to zero, indicating that the control system achieved its desired state quickly. This robust convergence behavior ensures successful enforcement of the sliding mode, providing a reliable and efficient control mechanism for the WECS.

4 Results and discussion

This section presents crucial simulation results that play a vital role in the design and implementation of a robust control technique for a WECS. We implement the controllers and the system model in MATLAB, connecting them using "goto" and "from" blocks. The simulation results demonstrate the effectiveness of FITSMC in accurately tracking the maximum power curve of the WECS. MATLAB simulations show the successful performance of the controller, ensuring precise speed tracking while incorporating the maximum power coefficient ($C_p = 0.4762$) and maintaining the tip speed ratio close to its optimal value ($\lambda = 7$). We conducted the simulations over a 50-s duration, considering an average wind speed of $v_w = 7\ m/s$.

Using the simulation results, we compare three control techniques: Feedback Linearization Control (FLC), Global Sliding Mode Control (GSMC), and finite-time integral terminal SMC. The main focus was on evaluating the tracking performance of the PMSG wind shaft speed with respect to the reference speed. Figures 3, 4 show the results of the performance evaluation. Figure 3 demonstrates that FITSMC outperformed GSMC in terms of the tracking performance. Additionally, Figure 4 illustrates the speed tracking error of the PMSG, showing that both the FLC and FITSMC, along with the GSMC, exhibit finite-time convergence.

In comparison to the FLC and GSMC, the FITSMC demonstrated a significant improvement in the tip speed ratio performance, as depicted in Figure 5. FITSMC exhibits reduced oscillation around the optimal tip speed ratio (λ_{opt}) and accurately tracks λ_{opt}, making it a promising candidate for achieving MPPT in variable-speed wind turbine systems.

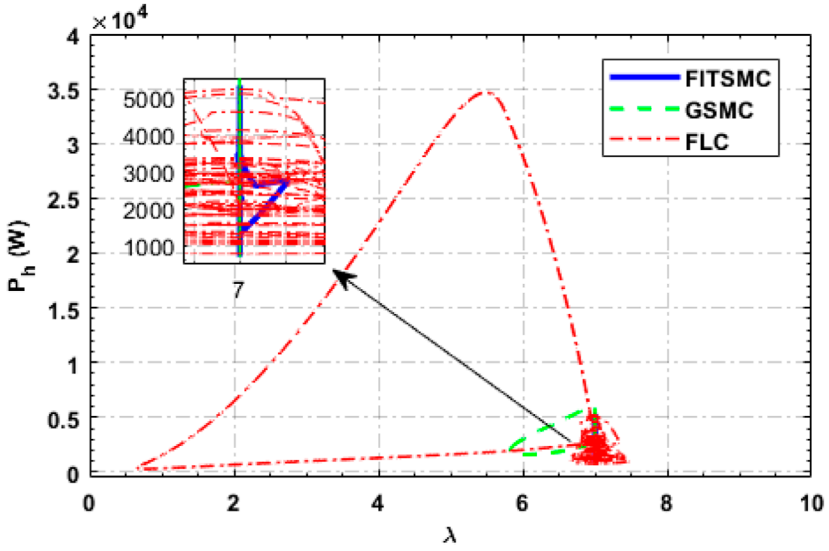

FIGURE 8
Variation of PMSG mechanical power with tip speed ratio.

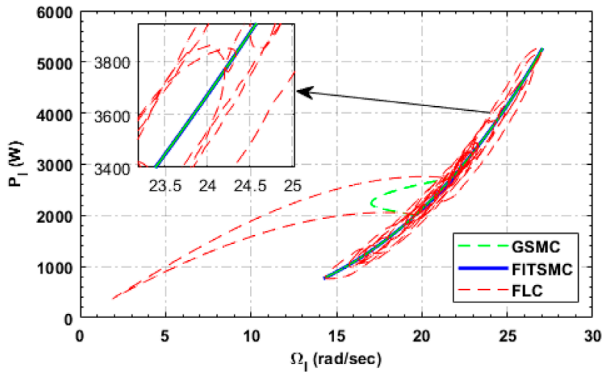

FIGURE 9
Relationship between wind turbine mechanical power and shaft speed.

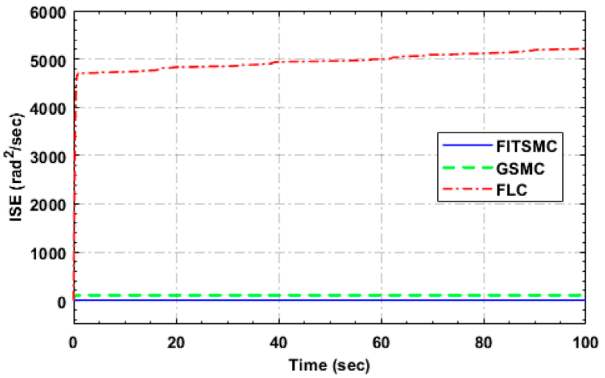

FIGURE 11
Integral squared error.

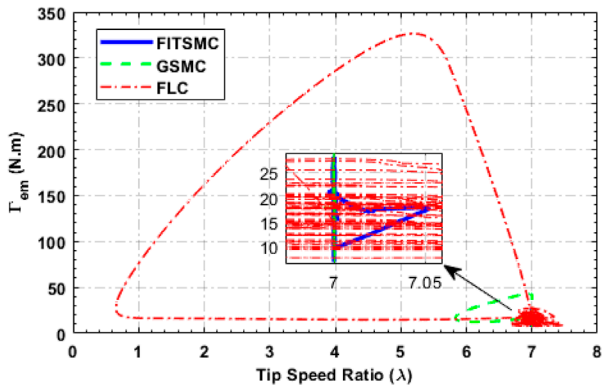

FIGURE 10
Variation of PMSG electromagnetic torque with tip speed ratio.

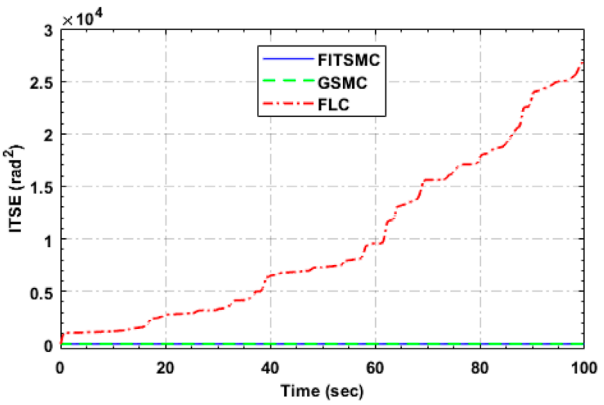

FIGURE 12
Integral of time squared error.

In Figure 6, FITSMC analyzes the power conversion coefficient of the VSWT and compares its results with those of the FLC and GSMC. FITSMC effectively tracks the optimal power conversion coefficient ($C_p = 0.4762$) throughout the stochastic wind speed profile, thereby ensuring efficient wind power extraction. The zoomed-in regions in Figure 6 visually represent FITSMC's exceptional tracking performance for $C_p(\max)$. The proposed MPPT strategy ensures highly efficient wind power extraction with minimal chattering, surpassing other MPPT approaches, such as FLC and GSMC. It precisely regulates the Tip Speed Ratio (TSR) at $\lambda_{opt} = 7$ and maintains the maximum power coefficient ($C_{p_{max}} = 0.4762$). Figures 7, 8 depict the development of the wind turbine and PMSG mechanical powers concerning the TSR, demonstrating the superior accuracy of the proposed MPPT paradigm in maintaining the TSR close to its optimal value. Moreover, Figure 9 shows the evolution of the wind turbine mechanical power as a function of its rotational speed, confirming the effectiveness of the proposed MPPT algorithm in continuously operating the WECS within the ORC to achieve maximum power extraction. In addition, Figure 10 emphasizes the PMSG electromagnetic torque development concerning the TSR, further underscoring the consistent ability of the proposed MPPT strategy to maintain the TSR around its optimal value, ensuring that the WECS extracts the maximum available power.

In the context of control system performance evaluation, various error metrics play a crucial role in assessing the effectiveness of a control strategy. For the system under study, it is essential to consider various aspects of the control performance. The significance of these error metrics is evident as follows: 1) The Integral Absolute Error (IAE) quantifies the magnitude of the absolute errors over a designated timeframe, offering valuable insights into the overarching capability of the control system for precise tracking. In the context of wind energy, precise tracking is crucial for maximizing energy production by ensuring that wind turbines operate near their maximum power point. A lower IAE indicates the proficiency of the control system in minimizing deviations from the desired performance. 2) The Integral Squared Error (ISE) and Integral Time Squared Error (ITSE) metrics emphasize minimizing both the error magnitude and its persistence over time. While IAE focuses on the absolute error magnitude, ISE and ITSE encompass squared errors accumulated over time. In the context of wind energy, reducing squared errors is critically important to mitigate the effects of prolonged performance deviations, which are vital for maintaining the stability and efficiency of wind turbines that operate continuously for extended periods. 3) The integral of the Time Absolute Error (ITAE) amalgamates both aspects of tracking precision (absolute error) and the control system's efficiency concerning the response time. In wind energy systems, achieving MPPT requires not only precision, but also rapid adaptation to changing wind conditions. ITAE quantifies overall control efficiency, considering both aspects.

In the context of control strategy performance, these error metrics become invaluable tools for assessment. Specifically, in the performance evaluation of the FITSMC control strategy, a comparison was made with the results obtained through two other control techniques, FLC and GSMC, via various error metrics, including ISE, ITSE, IAE, and ITAE. The simulation results, as illustrated in Figures 11–14, reveal how FITSMC excels in achieving

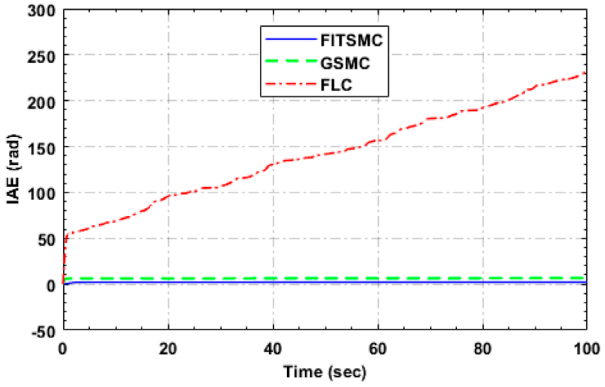

FIGURE 13
Integral absolute error.

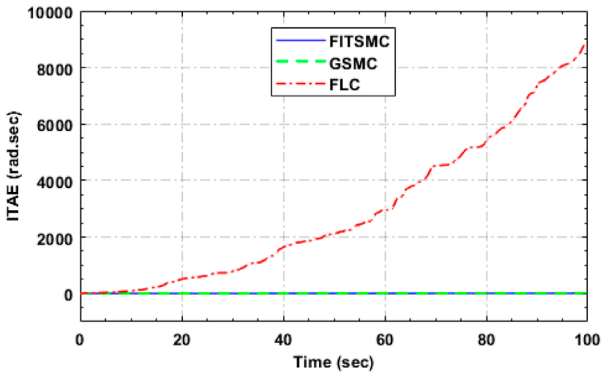

FIGURE 14
Integral of time absolute error.

precise tracking and finite-time convergence, while accumulating reduced errors over time. Through this comparison, it is evident that FITSMC outperforms both FLC and GSMC regarding tracking accuracy and efficiency, demonstrating the effectiveness of the control strategy in wind energy systems.

In summary, a comparative study between FITSMC, FLC, and GSMC provides valuable insights into the control and optimization of Wind Energy Conversion Systems. The FITSMC is a robust and efficient control technique that excels in tracking performance and MPPT capabilities. Its superiority makes it a promising option for enhancing the overall performance and efficiency of wind-energy conversion systems in practical applications. By employing the FITSMC, significant progress can be made in harnessing wind power effectively and promoting sustainability in the energy sector.

5 Conclusion

This paper presented a novel control approach, Finite-time Integral Terminal Sliding Mode Control, designed for standalone wind power systems to efficiently regulate wind turbine operation and maximize power extraction from wind energy. The FITSMC

strategy drives the system onto a sliding surface within a predefined terminal time, ensuring rapid convergence and overall stability. Extensive simulations demonstrated the robustness of the controller against uncertainties and disturbances, demonstrating its superiority over conventional methods in extracting the maximum power from wind resources. In future research, an extension of comparative analyses, optimization of FITSMC parameters, real-world experiments, integration of energy storage solutions, and exploration of AI-driven predictive control are envisioned to advance renewable energy technology and sustainability. These efforts are aimed at advance renewable energy technologies and sustainability.

Data availability statement

The raw data supporting the conclusions of this article will be made available by the authors, without undue reservation.

Author contributions

L-GH: Formal Analysis, Funding acquisition, Supervision, Investigation, Writing–review and editing. AA: Conceptualization, Data curation, Methodology, Software, Writing–original draft. SU: Conceptualization, Formal Analysis, Methodology, Project administration, Software, Supervision, Validation, Writing–original draft, Writing–review and editing. GH: Software, Supervision, Writing–review and editing. MZ: Formal Analysis, Investigation, Methodology, Writing–review and editing. LJ: Data curation, Funding acquisition, Validation, Writing–review and editing.

Funding

This research was funded by the Deanship of Scientific Research at King Khalid University. Dr. Monji Mohamed Zaidi, the Principal Investigator of the project, received a salary and provided financial support for this work through the Deanship of Scientific Research at King Khalid University. Dr. Monji also actively contributed to the research by collecting data, interpreting the results, and participating in reviewing the writing of the paper. Additionally, the authors acknowledge the Deanship of Scientific Research at King Khalid University for their support through large group Research Project grant (Grant Number: RGP2/105/44).

Acknowledgments

The authors extend their appreciation to the Deanship of Scientific Research at King Khalid University for funding this work through a large-group Research Project under grant number RGP2/105/44.

Conflict of interest

Authors L-GH and LJ are employed by PowerChina Huadong Engineering Corporation Limited, China.

The remaining authors declare that the research was conducted in the absence of any commercial or financial relationships that could be construed as a potential conflict of interest.

Publisher's note

References

Abdullah, M. A., Yatim, A., Tan, C. W., and Saidur, R. (2012). A review of maximum power point tracking algorithms for wind energy systems. *Renew. Sustain. energy Rev.* 16, 3220–3227. doi:10.1016/j.rser.2012.02.016

Aboudrar, I., El Hani, S., Heyine, M. S., and Naseri, N. (2019). Dynamic modeling and robust control by adrc of grid-connected hybrid pv-wind energy conversion system. *Math. Problems Eng. 2019* 2019, 1–19. doi:10.1155/2019/8362921

Alam, Z., Khan, Q., Khan, L., Ullah, S., Kirmani, S. A. M., and Algethami, A. A. (2022). Certainty-equivalence-based sensorless robust sliding mode control for maximum power extraction of an uncertain photovoltaic system. *Energies* 15, 2029. doi:10.3390/en15062029

Anjum, M. B., Khan, Q., Ullah, S., Hafeez, G., Fida, A., Iqbal, J., et al. (2022). Maximum power extraction from a standalone photo voltaic system via neuro-adaptive arbitrary order sliding mode control strategy with high gain differentiation. *Appl. Sci.* 12, 2773. doi:10.3390/app12062773

Chand, A., Khan, Q., Alam, W., Khan, L., and Iqbal, J. (2023). Certainty equivalence-based robust sliding mode control strategy and its application to uncertain pmsg-wecs. *Plos one* 18, e0281116. doi:10.1371/journal.pone.0281116

Cheikh, R., Menacer, A., Chrifi-Alaoui, L., and Drid, S. (2020). Robust nonlinear control via feedback linearization and lyapunov theory for permanent magnet synchronous generator-based wind energy conversion system. *Front. Energy* 14, 180–191. doi:10.1007/s11708-018-0537-3

Chu, W.-S., Chun, D.-M., and Ahn, S.-H. (2014). Research advancement of green technologies. *Int. J. Precis. Eng. Manuf.* 15, 973–977. doi:10.1007/s12541-014-0424-8

Costanzo, L., Schiavo, A. L., and Vitelli, M. (2019). Design guidelines for the perturb and observe technique for electromagnetic vibration energy harvesters feeding bridge rectifiers. *IEEE Trans. Industry Appl.* 55, 5089–5098. doi:10.1109/tia.2019.2923162

Cullen, R. A. (2000). What is maximum power point tracking (mppt) and how does it work? *Blue Sky Energy* 16.

Dali, A., Abdelmalek, S., Bakdi, A., and Bettayeb, M. (2021). A new robust control scheme: application for mpp tracking of a pmsg-based variable-speed wind turbine. *Renew. Energy* 172, 1021–1034. doi:10.1016/j.renene.2021.03.083

Hawkins, N., and McIntyre, M. L. (2021). A robust nonlinear controller for pmsg wind turbines. *Energies* 14, 954. doi:10.3390/en14040954

Jaramillo-Lopez, F., Kenne, G., and Lamnabhi-Lagarrigue, F. (2016). A novel online training neural network-based algorithm for wind speed estimation and adaptive control of pmsg wind turbine system for maximum power extraction. *Renew. Energy* 86, 38–48. doi:10.1016/j.renene.2015.07.071

Khan, I. U., Khan, L., Khan, Q., Ullah, S., Khan, U., and Ahmad, S. (2021). Neuro-adaptive backstepping integral sliding mode control design for nonlinearwind energy conversion system. *Turkish J. Electr. Eng. Comput. Sci.* 29, 531–547. doi:10.3906/elk-2001-113

Khan, M. A., Khan, Q., Khan, L., Khan, I., Alahmadi, A. A., and Ullah, N. (2022). Robust differentiator-based neurofuzzy sliding mode control strategies for pmsg-wecs. *Energies* 15, 7039. doi:10.3390/en15197039

Lee, C.-Y., Shen, Y.-X., Cheng, J.-C., Chang, C.-W., and Li, Y.-Y. (2009). Optimization method based mppt for wind power generators. *World Acad. Sci. Eng. Technol.* 60, 169–172. doi:10.5281/zenodo.1078400

Majout, B., Bossoufi, B., Bouderbala, M., Masud, M., Al-Amri, J. F., Taoussi, M., et al. (2022). Improvement of pmsg-based wind energy conversion system using developed sliding mode control. *Energies* 15, 1625. doi:10.3390/en15051625

Munteanu, I., Bratcu, A. I., Cutululis, N., and Ceanga, E. (2009). Optimal control of wind energy systems: towards a global approach. *IEEE control Syst. Mag.* doi:10.1007/978-1-84800-080-3

Pan, L., and Shao, C. (2020). Wind energy conversion systems analysis of pmsg on offshore wind turbine using improved smc and extended state observer. *Renew. Energy* 161, 149–161. doi:10.1016/j.renene.2020.06.057

Raj, T. G., and Kumar, B. R. (2018). "Comparative analysis of incremental conductance and perturb and observe mppt methods for single-switch dc/dc converter," in 2018 National Power Engineering Conference (NPEC) (IEEE), 1–5.

Saidi, Y., Mezouar, A., Miloud, Y., Kerrouche, K. D. E., Brahmi, B., and Benmahdjoub, M. A. (2020). Advanced non-linear backstepping control design for variable speed wind turbine power maximization based on tip-speed-ratio approach during partial load operation. *Int. J. Dyn. Control* 8, 615–628. doi:10.1007/s40435-019-00564-3

Soetedjo, A., Lomi, A., and Mulayanto, W. P. (2011). "Modeling of wind energy system with mppt control," in Proceedings of the 2011 International Conference on Electrical Engineering and Informatics (IEEE), 1–6.

Syahputra, R., and Soesanti, I. (2019). Performance improvement for small-scale wind turbine system based on maximum power point tracking control. *Energies* 12, 3938. doi:10.3390/en12203938

Tafticht, T., Agbossou, K., Cheriti, A., and Doumbia, M. (2006). "Output power maximization of a permanent magnet synchronous generator based stand-alone wind turbine," in *2006 IEEE international symposium on industrial electronics* (IEEE), 3, 2412–2416.

Ullah, A., Khan, L., Khan, Q., and Ahmad, S. (2020a). Variable gain high order sliding mode control approaches for pmsg basedvariable speed wind energy conversion system. *Turkish J. Electr. Eng. Comput. Sci.* 28, 2997–3012. doi:10.3906/elk-1909-69

Ullah, S., Khan, Q., and Mehmood, A. (2023). Neuro-adaptive fixed-time non-singular fast terminal sliding mode control design for a class of under-actuated nonlinear systems. *Int. J. Control* 96, 1529–1542. doi:10.1080/00207179.2022.2056514

Ullah, S., Mehmood, A., Ali, K., Javaid, U., Hafeez, G., and Ahmad, E. (2021). "Dynamic modeling and stabilization of surveillance quadcopter in space based on integral super twisting sliding mode control strategy," in 2021 International Conference on Artificial Intelligence (ICAI) (IEEE), 271–278.

Ullah, S., Mehmood, A., Khan, Q., Rehman, S., and Iqbal, J. (2020b). Robust integral sliding mode control design for stability enhancement of under-actuated quadcopter. *Int. J. Control, Automation Syst.* 18, 1671–1678. doi:10.1007/s12555-019-0302-3

Wang, J., Bo, D., Ma, X., Zhang, Y., Li, Z., and Miao, Q. (2019). Adaptive back-stepping control for a permanent magnet synchronous generator wind energy conversion system. *Int. J. hydrogen energy* 44, 3240–3249. doi:10.1016/j.ijhydene.2018.12.023

Zafran, M., Khan, L., Khan, Q., Ullah, S., Sami, I., and Ro, J.-S. (2020). Finite-time fast dynamic terminal sliding mode maximum power point tracking control paradigm for permanent magnet synchronous generator-based wind energy conversion system. *Appl. Sci.* 10, 6361. doi:10.3390/app10186361